Patterns formed by chains of magnetic beads

Danilo S. Borges[1,*], *Hans J.* Herrmann[1,2,**], *Humberto A.* Carmona[1,***], *José Soares* Andrade Jr.[1,****], and *Ascânio D.* Araújo[1,†]

[1]Departamento de Física, Universidade Federal do Ceará, Campus do Pici, 60455-760 Fortaleza, Ceará, Brazil
[2]PMMH, ESPCI, CNRS UMR 7636, 7 quai St. Bernard, 75005 Paris, France

Abstract. Magnetic beads attract each other forming rather stable chains. We consider such chains formed by magnetic beads and push them into a Hele-Shaw cell either from the boundary or from the center. When such a chain is pushed into a cavity, it bends and folds spontaneously forming interesting unreported patterns. These patterns are self-similar and an effective fractal dimension can be defined. As found experimentally and with numerical simulations, the numbers of beads, loops and contacts follow power laws as a function of packing fraction and, depending on the injection procedure, even energetically less favorable triangular configurations can be stabilized.

1 Introduction

Due to its many applications in mechanics and biology, the folding and crumpling of threads and wires is of increasing interest. A rich spectrum of patterns has been found depending on friction, stiffness, aspect ratio and the type of confinement [1]. Self-assembling systems like origamis have been devised by adding attractive forces [2]. Much less is known, however, when the wire has a chirality, as it is the case for a chain of magnetic particles. In fact, threads of magnetic beads can be found in Nature on different scales: on nanometric scale in magnetic colloids [3] and as chains of magnetosomes in magnetotactic bacteria [4]. Here we will consider macroscopic metal beads to study two-dimensional folding patterns by injecting them into a Hele-Shaw cell. Depending on the type of injection one can get two different folding orientations which then lead to completely distinct types of macroscopic patterns.

The injection of wires into cavities has been of interest to model the coiling of long DNA in globules and viral capsids [5] as well as a minimally invasive treatment of saccular aneurysms [6]. Fractal filling patterns have been observed, while the injection force diverges with a power law [7, 8]. Three different filling patterns have been observed depending on friction and the bending elasto/plasticity of the wire: a spiral phase, a folding phase and a chaotic phase [1, 9]. Also deformable cavities have been considered [10, 11]. Here we replace the wire by a chain of magnetic beads allowing for attractive and repulsive interactions between sections of the wire. This opens up a spectrum of new possibilities including the patterns, about which we will report here.

*e-mail: daniloborges@fisica.ufc.br
**e-mail: hans@fisica.ufc.br
***e-mail: carmona@fisica.ufc.br
****e-mail: soares@fisica.ufc.br
†e-mail: ascanio@fisica.ufc.br

A video is available at https://doi.org/10.48448/e18b-6663

2 Experiment

For the experiment we use magnetized neodymium beads of $d = 5$ mm diameter. The cavity consists of a flat acrylic cylinder of varying radius and 6 mm height put on a black dish and covered with a transparent plate of acrylic. Two step motors control the quasi-static (at 4.3 mm/s) injection into two diametrically opposed holes. Additionally, feeding into the center of the cavity through a hole in the bottom plate is possible. Images are recorded above the cavity with a digital camera Canon PowerShot SX510 HS in 30 frames per second at 23 cm and used to determine the particle positions. The magnetic beads naturally assemble with aligned dipole moments into wires that exhibit macroscopically elasto-plastic bending stiffness [12, 13]. These wires of beads are pushed into the cavity from opposite sides until the step motor is unable to proceed further. When the two chains come together they connect to each other (a little differently depending on the polarity of their tips). Typical patterns formed by the crumpling wires are shown in the lower row of Fig. 1*a*.

3 Results

Due to the attractive forces between opposite magnetic dipoles, neighboring chains tend to collapse into square lattice structures, which are energetically the most favorable configuration [13, 14] and the competition between this crystallization and the elastic bending forces of the chains produces the flower-like shapes seen in Fig. 1*a*. The network formed by contacting beads is shown for one pattern in Fig. 1*b*. Besides their compact core these patterns resemble the "classical" patterns of Ref. [1]. For our patterns the number of loops and the number of contacts increase with the packing fraction ϕ like power laws with exponents $\alpha = 1.72 \pm 0.06$ for loops and $\beta = 1.19 \pm 0.03$ for contacts, as shown in Fig. 2.

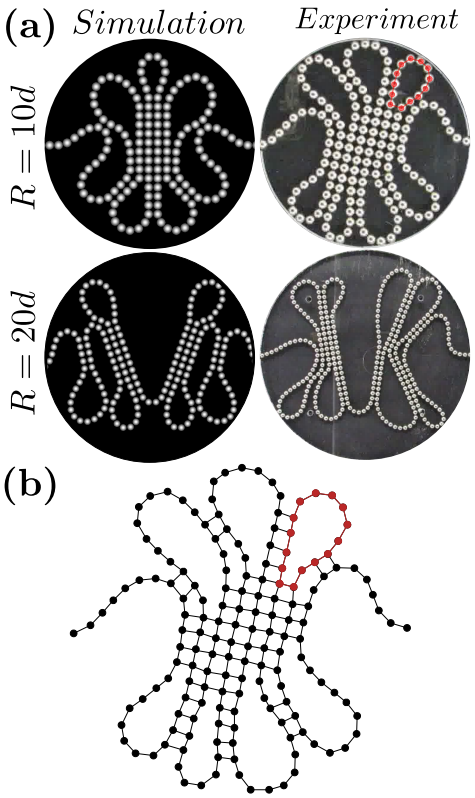

Figure 1. (a) Patterns obtained injecting wires of magnetic beads from opposite sides. First column: simulations using a molecular dynamics method (MD). Second column: experiments performed for two different cavity radii, namely, $R = 10d$ and $R = 20d$. (b) Contact network (graph) of the pattern obtained in a cavity of $R = 20d$ radius. Edges are established when the distance between the centers of the spheres are less than or equal to the sphere diameter. A typical loop is highlighted in red.

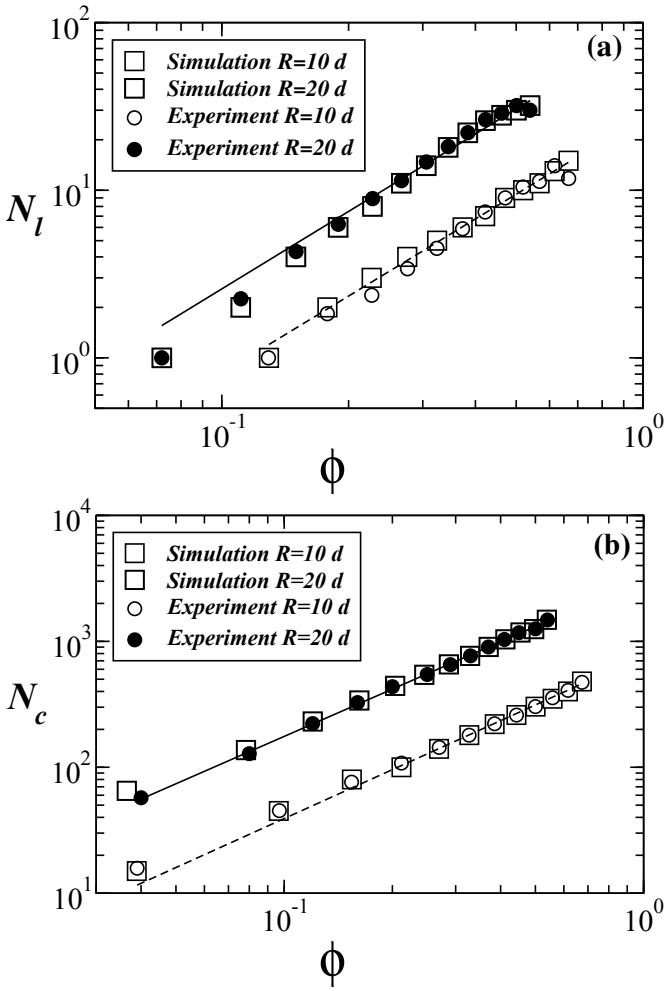

Figure 2. Log-log plot of (a) number of loops N_l and (b) number of contacts N_c as a function of the packing fraction ϕ. The open and full symbols correspond to a cavity of radius $R = 10d$ and $R = 20d$, respectively. The solid and dashed lines correspond to least-squares fits to the data, giving the scaling exponents $\alpha = 1.72 \pm 0.06$ for loops (a) and $\beta = 1.19 \pm 0.03$ for contacts (b).

If the radius of the cavity exceeds 25 particle diameters the two injected chains start to self-interact before reaching the opposite chain and the patterns become anisotropic. Beyond a radius of 40 particle diameters two separate aggregates independently grow on each side.

In order to characterize the aggregate morphology we choose the relationship between radius of gyration and number of beads to determine an effective "fractal dimension" [15–17],

$$R_g(N) \propto N^{1/d_f}$$

where $R_g(N)$ is the radius of a circle around the center and N the number of particles inside the circle. The average is taken over nine samples and the results can be seen in Fig. 3. Unfortunately, due to the small system sizes the range of validity of the power-law is too narrow to allow for the proper definition of a fractal dimension. From $R = 10d$ to $R = 20d$ the effective fractal dimension decreases from $d_f = 1.55 \pm 0.03$ to $d_f = 1.33 \pm 0.03$. For comparison, the fractal dimension found in Ref. [17] was $d_f = 1.54 \pm 0.03$ and $d_f = 1.71 \pm 0.01$ in Ref. [16].

Quite different is the situation when one chain is injected from the bottom into the center of the cavity as depicted in Fig. 4. We see that then eventually space is completely filled with beads. Besides their hexagonal texture these patterns resemble the "spiral" patterns found in Ref. [1]. What is spectacular about these compact patterns is their triangular crystallization, which clearly is energetically less favorable than the square lattice.

From the sequence of images in Fig. 4 we see that from the beginning, stripes of attached chains do not form squares as in Fig. 1, but triangles. By injecting from the bottom, the spheres in the chain and their magnetic moments undergo some rotations, which weakens their forces in the direction of the chain while allowing for out of plane interactions. As explained in Ref. [18] this favors a triangular lattice as shown in Figs. 5a and b.

In order to get a deeper understanding behind the energetic stability of the observed patterns we also performed Molecular Dynamics simulation. Short-range repulsions are accounted for through the repulsive part of a Lennard-Jones potential, while the magnetic pair forces $\boldsymbol{F}_{ij}$ and pair torques $\boldsymbol{\tau}_{ij}$ due to point-like magnetic dipoles at the centers of the beads are computed through

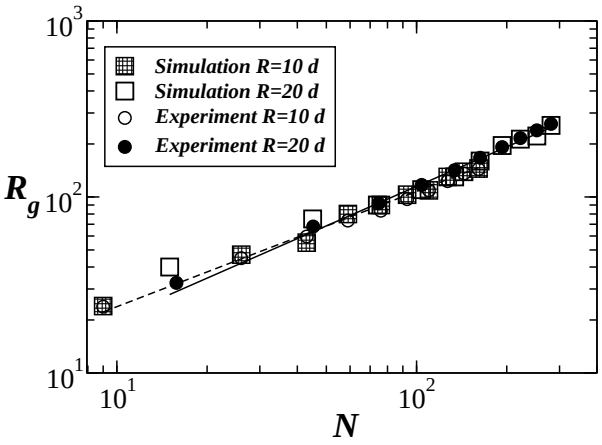

Figure 3. Radius $R_g(N)$ of a circle around the center versus the number N of particles inside the circle. The lines are least-squares fits to the data, giving the exponents $d_f = 1.55 \pm 0.04$ for $R = 10d$ (open circles) and $d_f = 1.34 \pm 0.03$ for $R = 20d$ (full circles).

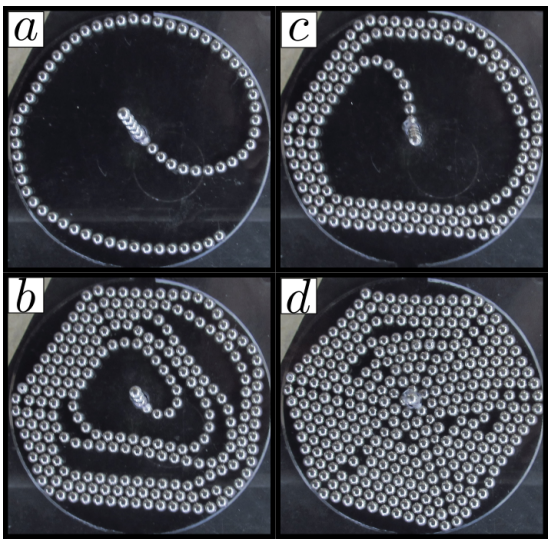

Figure 4. Four snapshots taken during the filling of the cavity. Here a chain of magnetic beads is injected into the cavity into the center from the bottom.

$$\boldsymbol{F}_{ij} = \boldsymbol{\nabla}\left(\boldsymbol{m}_i \cdot \boldsymbol{B}_j\right) \tag{1}$$

$$\boldsymbol{\tau}_{i,j} = \boldsymbol{m}_i \times \boldsymbol{B}_j \tag{2}$$

where

$$\boldsymbol{B}_j(\boldsymbol{r}_{ij}) = \frac{\mu_0}{4\pi}\left[\frac{3\left(\boldsymbol{m}_j \cdot \hat{\boldsymbol{r}}_{ij}\right)\hat{\boldsymbol{r}}_{ij} - \boldsymbol{m}_j}{r_{ij}^3}\right] \tag{3}$$

is the magnetic field produced by bead j at the position of bead i, $\boldsymbol{r}_{ij}$ is the vector pointing from the center of the bead i to the center of the bead j, $\hat{\boldsymbol{r}}_{ij} = \frac{\boldsymbol{r}_{ij}}{|\boldsymbol{r}_{ij}|}$ and μ_0 is the vacuum permeability.

The equations of motion for the translation and rotation of all beads, $\boldsymbol{F}_i = d\boldsymbol{p}_i/dt$ and $\boldsymbol{\tau}_i = d\boldsymbol{L}_i/dt$, were solved using a 6th order predictor-corrector method, where $\boldsymbol{p}_i$ and $\boldsymbol{L}_i$ are linear and angular momentum, respectively. After adjusting parameters we obtained simulated patterns that agree quite well with the experimental ones as seen in Fig. 1. We verified that our simulations also reproduce the experimental data quantitatively by calculating the number of loops and contacts as shown in Fig. 2 and the radius of gyration as shown in Fig. 3. Using the positions of the N beads from the simulation, the total magnetic potential energy E can be obtained by summing over all pairs of beads in the patterns according to Eq. (4).

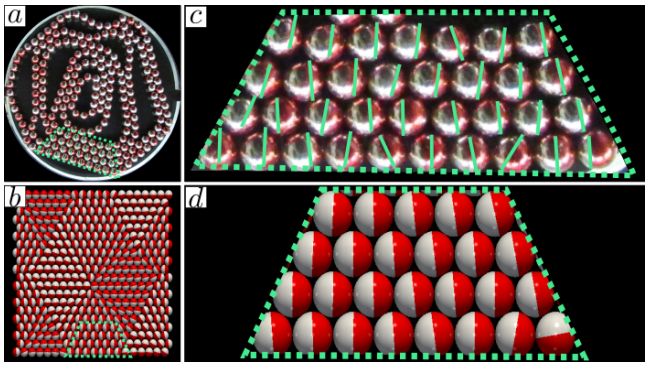

Figure 5. Lowest energy configuration of a triangular lattice for (*a*) experiment injecting the chain through the center of the cavity and (*b*) Monte Carlo simulation of dipoles on a triangular network with periodic boundary condition in both directions (top-bottom and right-left). Here, the dipoles can only rotate (not move) to reach the lowest energy configuration. In both cases, the dipoles are identified by painting in red the hemisphere (the heads of the dipoles) into which the dipole vector points. For the sake of clarity, we have added green lines along the direction of the dipoles on the experimental images as shown in (*c*). (d) For better visualization we magnify part of the Fig. 5 (b). We surround with a dashed green line a region of the packing, experimentally and numerically obtained where the magnetic dipole orientations exhibit considerable similarity. Those regions are shown in *c* and *d*, respectively. In these selected regions the pattern of the magnetic dipoles corresponds to the lowest energy configuration.

$$E = -\sum_{i=1}^{N-1}\sum_{j=i+1}^{N} \boldsymbol{m}_i \cdot \boldsymbol{B}_j \tag{4}$$

As seen in Fig. 6, for the case of flower-like patterns, we find that the total magnetic energy increases linearly with packing fraction, while the magnetic energy per particle tends to approximately $1.29E_0$, where $E_0 = -2\frac{\mu_0 m^2}{4\pi d^3}$ is the energy per particle for a pair of aligned dipoles of moment $\mathbf{m}$ separated by a distance d equal to the diameter of the beads.

On the square lattice, the configuration of the magnetic dipole moments with the lowest energy is very simple since it corresponds to the antiferromagnetic ground state of the Ising model. The situation on the triangular lattice is much more complicated, since it corresponds to the Heisenberg model on a triangular lattice which is known to be frustrated, exhibiting many ground states at low temperatures [19]. Fig. 5 shows that the lowest energy

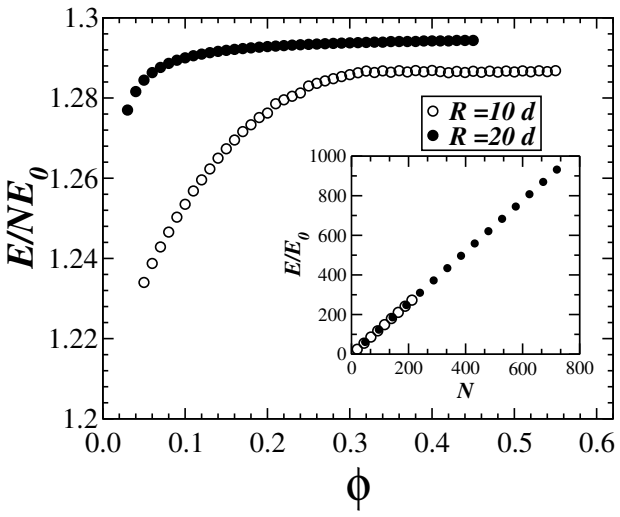

Figure 6. Total magnetic energy E normalized by E_0 (the minimum energy of a pair of dipoles of moment $\boldsymbol{m}$ at distance equal to the particle's radius) as a function of packing fraction obtained from the simulation. The simulation was performed for the flower-like pattern for two different cavity sizes, $R = 10d$ (open symbols) and $R = 20d$ (full symbols). The inset shows the energy density versus the packing fraction.

configurations on the triangular lattice involve magnetic dipole moments that are strongly aligned with the plane. To understand how the system evolves to the minimal energy configuration we realized a Monte Carlo simulation of dipoles on a triangular network with periodic boundary condition in both directions (top-bottom and right-left). Here, the dipoles can only rotate (not move) to reach the minimal energy configuration. As in the experiment, the results shown in Fig. 5*b* also reveal domains of parallel dipoles that are all rather strongly aligned with the plane of the cell. Once the metastable magnetic situation is locked in, the slight pressure pushing the chain against the cavity wall is sufficient to achieve the densest packing configuration and stabilize the pattern of Fig. 4. In fact, a transition to the flower-type pattern can be achieved by tilting the Hele-Shaw cell beyond the friction angle[18].

4 Conclusion

We have reported here new patterns that appear while feeding a chain of magnetic beads into a cavity. Precisely, if two chains are simultaneously injected from opposite sides, we observe flower-like structures having a square lattice in the center and loops as petals. If one chain is injected in the center, then the cavity is filled with a hexagon of six triangular lattices. We explained how this energetically metastable state can be attained.

We have shown with our model experiment how interactions between elements of a chain can modify its crumpling when injected into a cavity. This applies for instance to the coiling of long polymers in globules or viruses in capsids [5], which in fact not only exhibit magnetic effects but also many other types of interactions. Therefore, it would be interesting to also include electric, entropic, van der Waals and other forces in the future. It would also be important to study in the future the filling of three-dimensional cavities.

References

[1] N. Stoop, F.K. Wittel, H.J. Herrmann, Phys. Rev. Lett **101**, 094101 (2008)
[2] V.B. Shenoy, D.H. Gracias, MRS Bull. **37**, 847 (2012)
[3] L.J. Hill, J. Pyun, ACS Appl. Mat. & Interfaces **6**, 6022 (2014)
[4] V.P. Shcherbakov, M. Winklhofer, M. Hanzlik, N. Petersen, Europ. Biophys. J. **26**, 319 (1997)
[5] K.E. Richards, R.C. Williams, R. Calendar, J. Mol. Biol. **78**, 255 (1973)
[6] S.C. Johnston et al., Stroke **33**, 2536 (2002)
[7] C.C. Donato, M.A.F. Gomes, R.E. de Souza, Phys. Rev. E **66**, 015102 (2002)
[8] Y.C. Lin, Y.W. Lin, T.M. Hong, Phys. Rev. E **78**, 067101 (2008)
[9] R. Vetter, F.K. Wittel, N. Stoop, H.J. Herrmann, Eur. J. Mech **37**, 160 (2013)
[10] R. Vetter, F.K. Wittel, H.J. Herrmann, Nat. Comm. **5**, 4437 (2014)
[11] H. Elettro, F. Vollrath, A. Antkowiak, S. Neukirch, Soft Matter **13**, 5509 (2017)
[12] C.L. Hall, D. Vella, A. Goriely, SIAM J. Appl. Math. **73**, 2029 (2013)
[13] D. Vella, E. du Pontavice, C.L. Hall, A. Goriely, J. Appl. Math. **470**, 20130609 (2014)
[14] H. Schmidle, C.K. Hall, O.D. Velev, S.H.L. Klapp, Soft Matter **8**, 1521 (2012)
[15] T. Vicsek, *Fractal growth phenomena* (World Scientific, Singapore, 1992)
[16] R. Pastor-Satorras, J.M. Rubí, *Trends in Colloid and Interface Science XII* (Springer, 1998) 29-33
[17] J. Byrom, S.L. Biswal, Soft Matter **9**, 9167 (2013)
[18] D.S. Borges, H.J. Herrmann, H.A. Carmona, J.S. Andrade Jr., A.D. Araújo, Phys. Rev. Lett. **126**, 118001 (2021)
[19] F.L. Buessen, M. Hering, J. Reuther, S. Trebst, Phys. Rev. Lett. **120**, 057201 (2018)